NASA CR - 112231

A PARAMETRIC STUDY OF PLANFORM AND AEROELASTIC EFFECTS ON AERODYNAMIC CENTER, a- AND q- STABILITY DERIVATIVES

APPENDIX C

METHOD FOR COMPUTING THE AERODYNAMIC INFLUENCE COEFFICIENT MATRIX OF NONPLANAR WING-BODY-TAIL CONFIGURATIONS

by
J. Roskam, C. Lan, and S. Mehrotra

CRINC-FRL 72-013

October 1972

Prepared under NASA Grant NGR 17-002-071 by
The Flight Research Laboratory
Department of Aerospace Engineering
The University of Kansas
Lawrence, Kansas 66044
for
Langley Research Center
National Aeronautics and Space Administration

TABLE OF CONTENTS

1. INTRODUCTION

The purpose of this appendix is to derive expressions for computing the Aerodynamic influence coefficient matrix (or [A] matrix) for nonplanar wing-body-tail configurations. An aerodynamic influence coefficient a_{ij} (i.e. an element of the A matrix) is defined as the load in lbs. (Newtons) induced on panel i as a result of a unit angle of attack (rad) on panel j. Simulation of wing-body interference is not attempted. Fuselage, wing and tail thickness are assumed to be small with the result that the thickness effect on the flow-field is negligible. No dihedral effects are considered, even though these can be easily included by computing both downwash and sidewash. Camber effects may also be included. Symbols used in this appendix are defined in Section 2.

The method for determining the aerodynamic influence coefficient matrix is based on the "lifting" solution to the small perturbation, steady potential flow equation. Expressions for the various velocity functions, needed for computing the downwash are presented in Section 3 of this appendix. In section 4, a comparison of pressure distributions and stability derivatives derived from this investigation, with already existing results is made.

2. SYMBOLS

The units used for the physical quantities defined in this paper are given both in the International System of Units (SI) and the U.S. Customary Units.

Symbol	Description	Dimension
a	Downwash influence coefficient	Nondimensional
$[A]$	Aerodynamic influence coefficient	$ft^2\ rad^{-1}$ ($m^2\ rad^{-1}$)
AR	Aspect ratio	Nondimensional
b'_{jk}	L_{jk}/β	Nondimensional
C_P	Pressure coefficient	Nondimensional
F_A	Aerodynamic Pressure force on a panel	Lbs. (Newton)
F	Velocity function	Nondimensional
K	Constant	
L	Slope of leading or trailing edges of a panel	Nondimensional
M_∞	Free stream Mach number	Nondimensional
$\bar{q}$	Dynamic pressure	Lbs. ft^{-2} (Newton m^{-2})
S	Area of a panel	ft^2 (m^2)
u	Perturbation velocity in x-direction	Nondimensional
v	Perturbation velocity in y-direction	Nondimensional
w	Perturbation velocity in z-direction, downwash	Nondimensional
(x, y, z)	Rectangular Cartesian coordinate system	ft. (m)
Z_c	Ordinates of Camber line	ft. (m)

Symbol	Description	Dimensional
Greek		
α	Angle of attack	rad
α_w	$= (\alpha - \frac{dZ_c}{dx})$	rad
β	$= \sqrt{\lvert M_\infty{}^2 - 1 \rvert}$	Nondimensional
ϕ	Velocity potential	Nondimensional
(ξ, η)	Integration variables in Cartesian system	ft. (m)
$\eta = \frac{Y}{b/2}$	Spanwise station in fraction of the semi-span	
Subscripts		
i	Aerodynamic panel number	
j	Aerodynamic panel number	
k	Panel corner point	
k	Aerodynamic panel number	
$(\ )'$	Referred to primed system of coordinates	
Matrices		
$[\ ]$	Square matrix (n x n)	
$\{\ \}$	Column matrix (n x 1)	
$\{\ \}^T$	Row matrix (1 x n)	
$[\searrow]$	Diagonal matrix (n x n)	

3. METHOD OF ANALYSIS

The aerodynamic influence coefficient method is based on the "lifting" solution to the small perturbation, steady potential flow equation:

$$(1 - M_\infty^2)\,\phi_{xx} + \phi_{yy} + \phi_{zz} = 0 \tag{1}$$

where ϕ is the perturbation velocity potential and M_∞ the freestream Mach number. Note that the same equation is also satisfied by the perturbed velocity components. It is well known that the lifting solution of the above equation can be obtained with a vortex distribution with strength to be determined by satisfying a boundary condition of flow tangency on the wing surface. In this appendix the Woodward's method of solution (Reference 1), has been used.

In Woodward's method, the entire wing or airplane planform is divided into a number of quadrilateral panels as shown in Figure (1). On each panel, the incidence and camber effects are represented by a constant planar pressure vortex distribution with an unknown strength Δu. The velocity potential at any point in the flow field due to this vortex distribution on one panel is given by:

$$\phi(x', y', z') = \frac{K\Delta u}{2\pi} \iint_{\text{Panel}} \frac{z'(x' - \xi)\, d\xi d\eta}{[(y' - \eta)^2 + z'^2]\sqrt{(x' - \xi)^2 + (1-M_\infty^2)\,[(y' - \eta)^2 + z'^2]}}$$

$$+ \frac{(1 - K)\Delta u}{2\pi} \iint \frac{z' d\xi d\eta}{(y' - \eta)^2 + z'^2} \tag{2}$$

where $K = 0.5$ for $M_\infty < 1$ and $K = 1.0$ for $M_\infty > 1$. The primed coordinate system is a local coordinate system as shown in Figure (2). There are many ways of finding the integrals in Equation (2). A simple way is to regard each panel as an algebraic sum of four semi-infinite triangular regions as shown in Figure (3a).

Thus, the velocity potential at any point P is given by:

$$\phi(P) = \phi_1 \text{ (semi-infinite triangular region from corner 1)}$$

$$- \phi_2 \text{ (semi-infinite triangular region from corner 2)}$$

$$- \phi_3 \text{ (semi-infinite triangular region from corner 3)}$$

$$+ \phi_4 \text{ (semi-infinite triangular region from corner 4)}$$

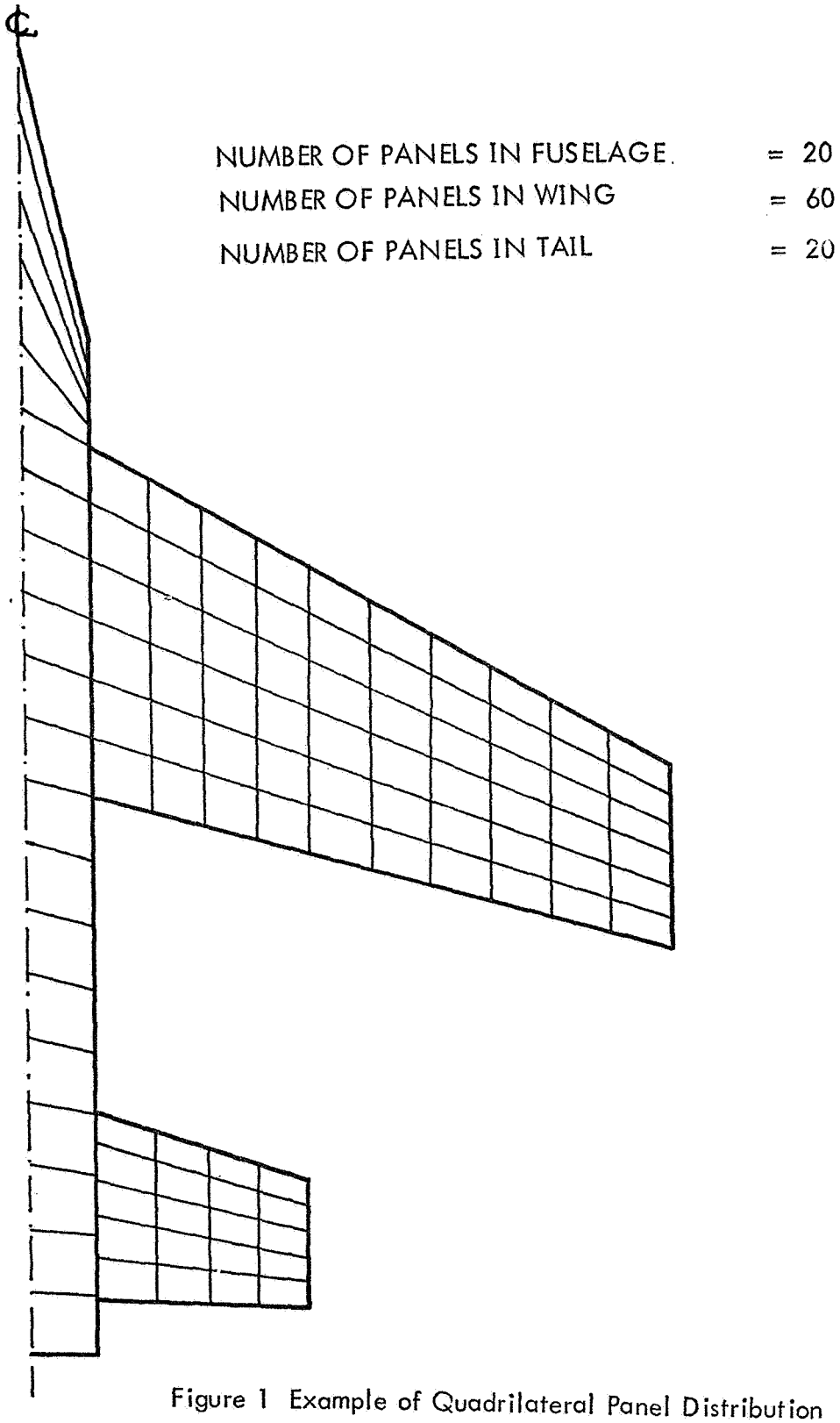

Figure 1 Example of Quadrilateral Panel Distribution

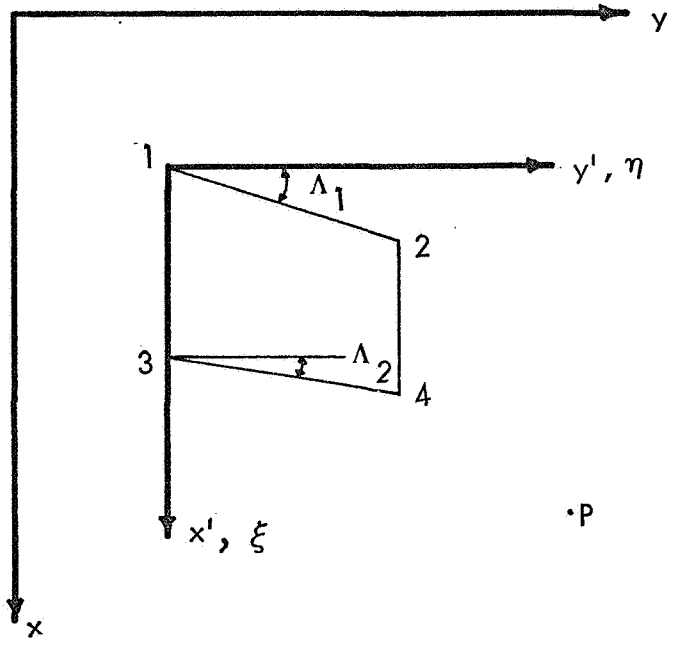

Figure 2 Definition of Panel Coordinate System

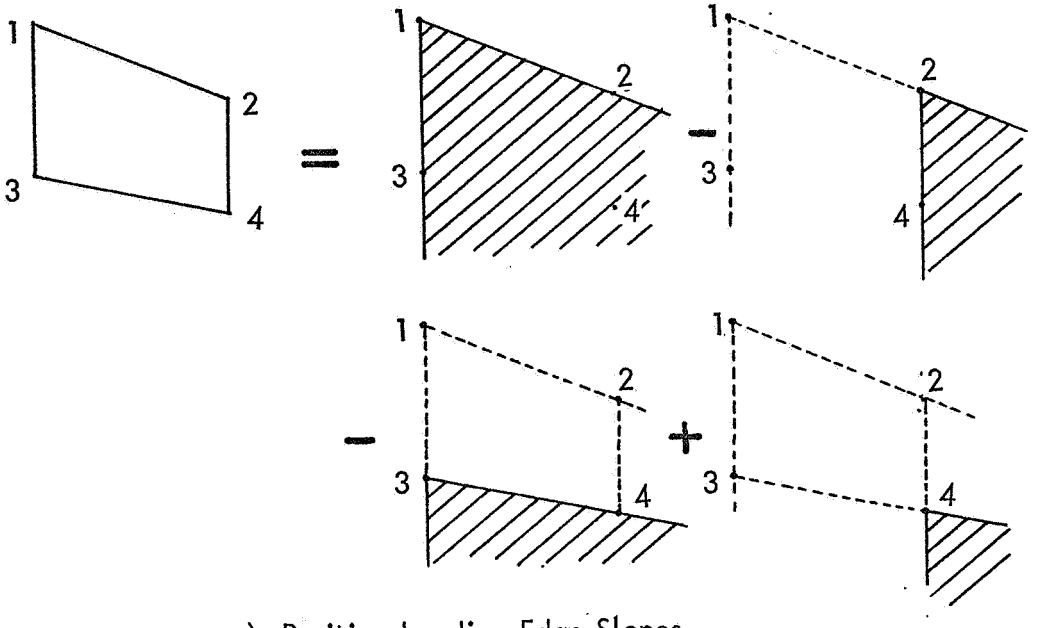

a) Positive Leading Edge Slopes

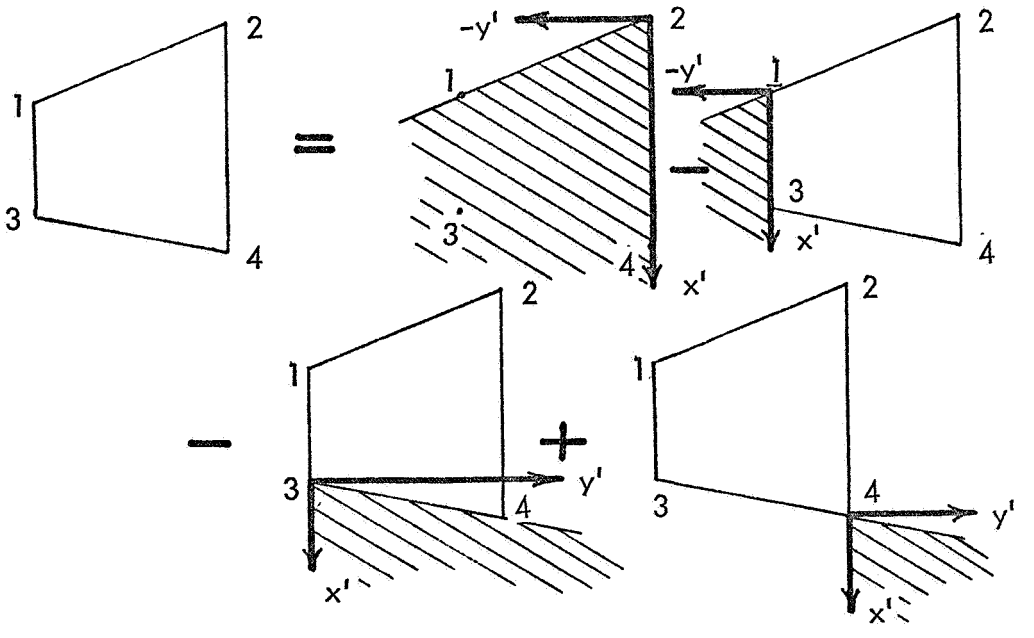

b) Negative Leading Edge Slopes

Figure 3 Decomposition of Area of Integration

A similar approach can also be used when the leading and trailing edges of the panel have negative slopes and when points 2 and 4 are coincident, i.e., the panel is triangular. In the latter case, the same scheme as for the positive leading edge shape can be used. However, when the leading edge slope is negative, the scheme shown in Figure (3b) is convenient.

It is clear then that the fundamental region of integration for Equation (2) is the semi-infinite triangular region with a positive leading edge slope. If the equation of the leading edge is given by $\xi = L\eta$, the velocity potential due to a constant pressure vortex distribution in the semi-infinite triangular region from the corner k is as follows:

$$\phi_k = \frac{K\Delta u}{2\pi} \int_o^{\eta_1} d\eta \int_{L\eta}^{\xi_1} \frac{z' (x' - \xi)\, d\xi\, d\eta}{[(y' - \eta)^2 + z'^2]\sqrt{(x' - \xi)^2 + (1-M_\infty^2)[y' - \eta)^2 + z'^2]}}$$

$$+ \frac{(1 - K)\Delta u}{2\pi} \int_o^{\eta_1} d\eta \int_{L\eta}^{\xi_1} \frac{z'\, d\xi\, d\eta}{(y' - \eta)^2 + z'^2} \qquad (3)$$

where $x' = x_p - x_k$, $y' = y_p - y_k$ and $z' = z_p$. In subsonic flow, $\xi_1 = \infty$ and $\eta_1 = \infty$. In supersonic flow, the integration limits are as shown in Figure (4) and are given below:

$$\xi_1 = x' - \{(M_\infty^2 - 1)\ [(y' - \eta)^2 + z'^2]\}^{1/2} \qquad (3a)$$

$$\eta_1 = \frac{Lx' - (M_\infty^2 - 1)^{1/2}\, y' - \{(M_\infty^2 - 1)\ [(x' - Ly')^2 + (L^2 + 1 - M_\infty^2)\, z'^2]\}^{1/2}}{L^2 + 1 - M_\infty^2} \qquad (3b)$$

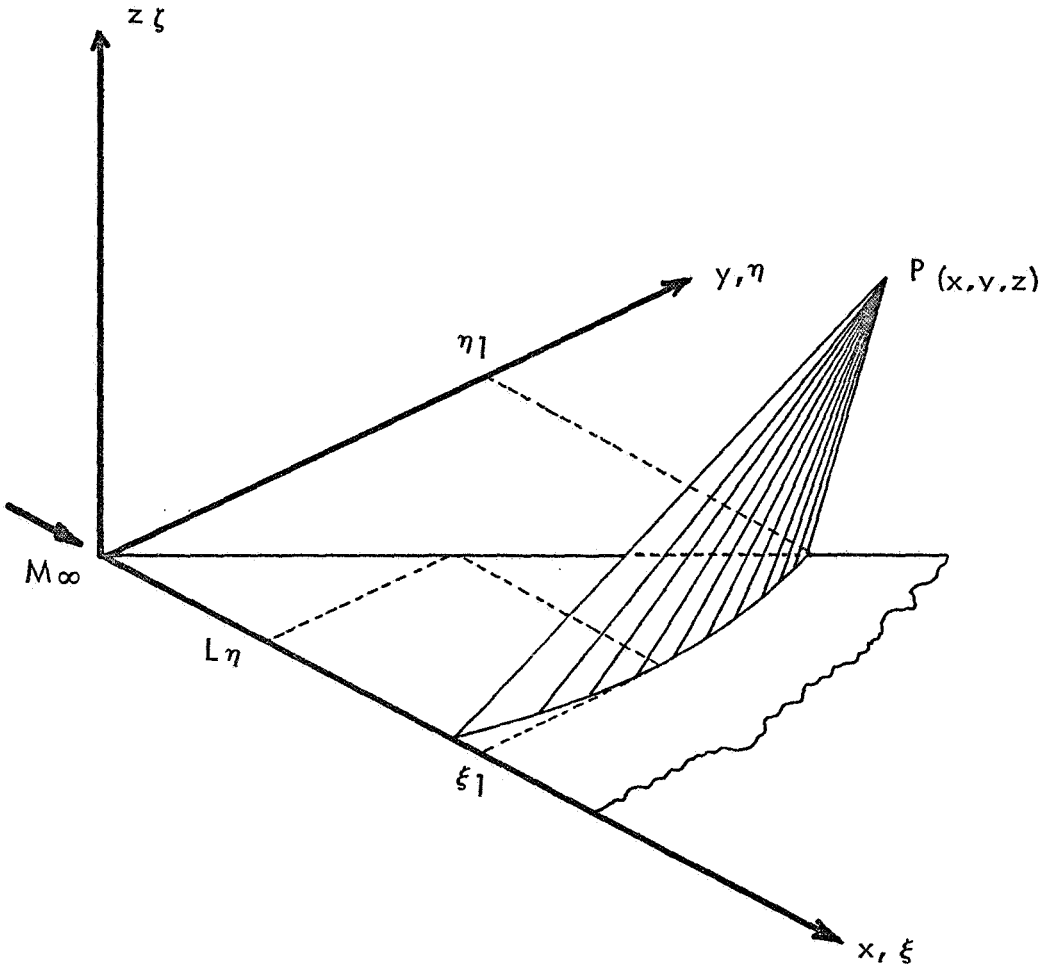

Figure 4 Limits of Integration in Supersonic Flow

Equations (3) have been integrated in closed form by Woodward (Reference 1) The result is:

$$\phi_k = \frac{K\Delta u}{2\pi} \left\{ (x' - Ly') (F_3 + F_4) + z' \left[(L^2 + 1 - M_\infty^2) \frac{F_2}{\beta} - L (F_1 - F_5) \right] \right\} \tag{4}$$

The corresponding velocity components are:

$$u_k (p) = \frac{\partial \phi_k}{\partial x_p} = \frac{K\Delta u}{2\pi} (F_3 + F_4)$$

$$v_k (p) = \frac{\partial \phi_k}{\partial y_p} = \frac{K\Delta u}{2\pi} \left[L (F_3 + F_4) - z'\beta F_6 \right] \tag{5}$$

$$w_k (p) = \frac{\partial \phi_k}{\partial z_p} = \frac{K\Delta u}{2\pi} \left[\frac{L^2 + 1 - M_\infty^2}{\beta} F_2 - L (F_1 - F_5) - y'\beta F_6 \right]$$

The velocity functions F's are defined as follows:

$$F_1 = \text{Re} \left\{ \log \frac{x' + d'}{\sqrt{\left| 1 - M_\infty^2 \right|}\, r'} \right\} \tag{6a}$$

$$F_2 = \beta \ \text{Re} \left\{ \log \frac{\tilde{x} + \tilde{d}}{\sqrt{\left| 1 - M_\infty^2 \right|}\, r'} \right\} \Bigg/ (L^2 + 1 - M_\infty^2)^{1/2} \tag{6b}$$

$$F_3 = \text{Re} \left\{ \tan^{-1} \frac{z'd'}{Lr'^2 - x'y'} \right\} \tag{6c}$$

$$\left.\begin{aligned} F_4 &= \tan^{-1} \frac{y'}{z'} \qquad \text{for } M_\infty < 1 \\ F_4 &= 0 \qquad \text{for } M_\infty \geq 1 \end{aligned}\right\} \tag{6d}$$

$$F_5 = \log \frac{Lr'}{r} \quad \text{for } M_\infty \leq 1$$

$$F_5 = 0 \quad \text{for } M_\infty > 1 \qquad (6e)$$

$$F_6 = \frac{x' + d'}{\beta r'^2} \quad \text{for } M_\infty \leq 1$$

$$F_6 = \frac{d'}{\beta r'^2} \quad \text{for } M_\infty > 1 \qquad (6f)$$

where:

$$r' = (z'^2 + y'^2)^{1/2} \qquad (7a)$$

$$d' = [x'^2 + (1 - M_\infty^2)\, r'^2]^{1/2} \qquad (7b)$$

$$\tilde{x} = Lx' + (1 - M_\infty^2)y' \qquad (7c)$$

$$\tilde{y} = x' - Ly' \qquad (7d)$$

$$\tilde{r} = [(x' - Ly')^2 + (L^2 + 1 - M_\infty^2)z'^2]^{1/2} \qquad (7e)$$

$$\tilde{d} = [\tilde{x}^2 + (1 - M_\infty^2)\, \tilde{r}^2]^{1/2} \qquad (7f)$$

$$\beta = \sqrt{|1 - M_\infty^2|} \qquad (7g)$$

Let p be the downwash control point of a panel. Then the downwash at p of panel i due to a unit vortex distribution on the semi-infinite triangular region from the corner k of panel j is given by:

$$w_{ijk}(p) = \frac{K\beta}{2\pi} \left\{ (b'^2_{jk} \pm 1) F_2(ijk) - b'_{jk} [F_1(ijk) - F_5(ijk)] - y'_{ijk} F_6(ijk) \right\} \qquad (8)$$

where the plus sign is for the subsonic case and the minus sign for the supersonic case. The quantities b'_{jk} and y'_{ijk} in Equation (8) are defined as follows:

$$b'_{jk} = \frac{L_{jk}}{\beta} = \frac{1}{\beta}\,\frac{x_{j2} - x_{j1}}{y_{j2} - y_{j1}} \qquad \text{for } k = 1, 2$$

$$= \frac{1}{\beta}\,\frac{x_{j4} - x_{j3}}{y_{j4} - y_{j3}} \qquad \text{for } k = 3, 4 \qquad (9)$$

$$y'_{ijk} = y_i - y_{jk} \qquad (10)$$

x'_{ijk} and z'_{ijk} can also be defined in a similar way as:

$$x'_{ijk} = x_i - x_{jk} \qquad (11)$$

$$z'_{ijk} = z_i - z_{jk} \qquad (12)$$

and also

$$\xi'_{jk} = \frac{x'_{ijk}}{\beta} \qquad (13)$$

Equation 8 indicates that only F_1, F_2, F_5 and F_6 velocity functions are needed to evaluate the downwash w_k. Simplified expressions of these velocity functions can be derived by using equations 7 and 9 through 13. These expressions for both subsonic and supersonic cases are presented in Table 1.

Referring back to equation 8, it follows that the downwash at point p of panel i due to a unit vortex distribution on the jth panel, represented by a_{ij1}, can be written as:

$$a_{ij1} = w_{ij1} - w_{ij2} - w_{ij3} + w_{ij4} \qquad (18)$$

In this report only symmetric flight configurations are considered. Let the mirror image of the jth panel with respect to the line of symmetry be denoted by j'^{th} panel. The downwash at point p due to the panel j' is a_{ij2}. The total downwash at p due to a unit vortex distribution on both j^{th} and j'^{th} panels is then:

$$a_{ij} = a_{ij1} + a_{ij2} \qquad (19)$$

Table 1 Velocity functions for computing downwash according to equation 8

Subsonic Case:

$$F1 = \mathrm{Re}\ \ln\left(\frac{x' + d'}{|\beta|\, r'}\right)$$

$$= \ln\left(\frac{\xi' + \sqrt{\xi'^2 + y'^2 + z'^2}}{\sqrt{y'^2 + z'^2}}\right) \tag{14a}$$

$$F2 = \mathrm{Re}\ \frac{\beta}{\sqrt{L^2 + \beta^2}}\ \ln\left(\frac{\tilde{x} + \tilde{d}}{|\beta|\,\tilde{r}}\right)$$

$$= \frac{1}{\sqrt{b'^2 + 1}}\ \ln\left(\frac{y' + b'\xi' + \sqrt{(y' + b'\xi')^2 + (\xi' - b'y')^2 + (b'^2 + 1)z'^2}}{\sqrt{(\xi' - b'y')^2 + (b'^2 + 1)z'^2}}\right) \tag{14b}$$

$$F5 = \ln\left(\frac{Lr'}{\tilde{r}}\right)$$

$$= \ln\left(\frac{|b'|\sqrt{y'^2 + z'^2}}{\sqrt{(\xi' - b'y')^2 + (b'^2 + 1)z'^2}}\right) \tag{14c}$$

$$F6 = \frac{(x' + d')}{\beta\, r'^2}$$

$$= \frac{\xi' + \sqrt{\xi'^2 + y'^2 + z'^2}}{(y'^2 + z'^2)} \tag{14d}$$

Supersonic Case:

Case 1. $\xi' > \sqrt{y'^2 + z'^2}$

$$F1 = \ln\left(\frac{\xi' + \sqrt{\xi'^2 - (y'^2 + z'^2)}}{\sqrt{y'^2 + z'^2}}\right) \tag{15a}$$

$$F2 = \frac{1}{\sqrt{b'^2 - 1}} \ln\left(\frac{(b'\xi' - y') + \sqrt{(b'\xi' - y')^2 - \left((\xi - b'y')^2 + (b'^2 - 1)\, z'^2\right)}}{(\xi' - b'y')^2 + (b'^2 - 1)\, z'^2}\right),$$

$$\underline{\text{if } b' > 1} \tag{15b}$$

$$= \sqrt{\frac{\xi'^2 - y'^2 - z'^2}{(\xi' - y')}}, \quad \underline{\text{if } b' = 1} \tag{15c}$$

$$F2 = \frac{1}{\sqrt{1 - b'^2}} \cos^{-1}\left(\frac{(b'\xi' - y')}{\sqrt{(\xi' - b'y')^2 + (b'^2 - 1)z'^2}}\right), \quad \underline{\text{if } b' < 1} \tag{15d}$$

$$F5 = 0 \tag{15e}$$

$$F6 = \frac{\sqrt{\xi'^2 - y^2 - z'^2}}{(y'^2 + z'^2)} \tag{15f}$$

Case 2. $\xi' = \sqrt{y'^2 + z'^2}$ and $b' < 1$

$$F1 = 0 \tag{16a}$$

$$F2 = 0 \qquad \underline{\text{if } y' < b'\xi'} \tag{16b}$$

$$F2 = \frac{\pi}{2\sqrt{1 - b'^2}}, \qquad \underline{\text{if } y' = b'\xi'} \tag{16c}$$

$$F2 = \frac{\pi}{\sqrt{1 - b'^2}}, \qquad \underline{\text{if } y' > b'\xi'} \tag{16d}$$

$$F5 = 0 \tag{16e}$$

$$F6 = 0 \tag{16f}$$

Note: If $\xi' = \sqrt{y'^2 + z'^2}$ and $b' \geq 1$, all functions are zero.

Case 3. $\xi' < \sqrt{y'^2 + z'^2}$ and $b' < 1$.

$$F1 = 0. \tag{17a}$$

$$F2 = 0. \qquad \text{if } y' \leq 0 \tag{17b}$$

$$F2 = 0 \qquad \text{if } y' > 0 \text{ and } \xi' < (b'y' + \sqrt{1 - b'^2}\,|z'|) \tag{17c}$$

$$F2 = \frac{\pi}{2\sqrt{1 - b'^2}} \qquad \text{if } y' > 0 \text{ and } \xi' = (b'y' + \sqrt{1 - b'^2}\,|z'|) \tag{17d}$$

$$F2 = \frac{\pi}{\sqrt{1 - b'^2}} \qquad \text{if } y' > 0,\ \xi' > (b'y' + \sqrt{1 - b'^2}\,|z'|) \text{ and } y' > b'\xi' \tag{17e}$$

$$F2 = \frac{\pi}{2\sqrt{1 - b'^2}} \qquad \text{if } y' > 0,\ \xi' > (b'y' + \sqrt{1 - b'^2}\,|z'|) \text{ and } y' = b'\xi' \tag{17f}$$

$$F2 = 0 \qquad \text{if } y' > 0,\ \xi' > (b'y' + \sqrt{1 - b'^2}\,|z'|) \text{ and } y' < b'\xi' \tag{17g}$$

$$F5 = 0. \tag{17h}$$

$$F6 = 0. \tag{17i}$$

Note: If $\xi' < \sqrt{y'^2 + z'^2}$ and $b' \geq 1$, all functions are zero.

The boundary conditions require that the flow be tangential to the camber line. Since the downwash at p of panel i due to the vortex distribution on all panels is:

$$\sum_{j=1}^{N_w} a_{ij} \, (\Delta u)_j$$

where N_w is the number of panels on one-half of the wing, fuselage and tail, the tangency condition can be written as:

$$\left(\frac{dz_c}{dx} - \alpha \right)_i = \sum_{j=1}^{N_w} a_{ij} \, (\Delta u)_j \qquad (20)$$

or in matrix form:

$$\left\{ \frac{dz_c}{dx} - \alpha \right\} = [a_{ij}] \{\Delta u\} \qquad (21)$$

Solving this equation for $\{\Delta u\}$, the unknown vortex strengths Δu are obtained as:

$$\{\Delta u\} = [a_{ij}]^{-1} \left\{ \frac{dz_c}{dx} - \alpha \right\} . \qquad (22)$$

Note that $\Delta u = u^+ - u^-$. Since $C_p = -2u$, it follows that $\Delta C_p = C_p^- - C_p^+ = 2\Delta u$.

Hence:

$$\{\Delta C_p\} = 2 \, [a_{ij}]^{-1} \left\{ \frac{dz_c}{dx} - \alpha \right\} \qquad (23)$$

The total force on any panel i is given by:

$$F_{A_i} = \bar{q} S_i \, (\Delta C_{p_i}) \qquad (24)$$

where S_i is the area of panel i and $\bar{q}$ is the dynamic pressure. In matrix form, the panel forces can be written as:

$$\{F_A\} = \bar{q} \begin{bmatrix} S_1 & & 0 \\ & S_2 & \\ & \ddots & \\ 0 & & S_{N_w} \end{bmatrix} \{\Delta C_p\}$$

$$= 2\bar{q} \begin{bmatrix} \diagdown S \diagup \end{bmatrix} [a_{ij}]^{-1} \left\{ \frac{dz_c}{dx} - \alpha \right\}$$

$$= \bar{q} \; [A] \; \{\alpha_w\} \tag{25}$$

Where $[A]$ is the aerodynamic influence coefficient matrix and is given by:

$$[A] = -2 \begin{bmatrix} \diagdown S \diagup \end{bmatrix} [a_{ij}]^{-1} \tag{26}$$

and

$$\alpha_w = \alpha - \frac{dz_c}{dx} \tag{27}$$

The computer program for generating this $[A]$ matrix is included in Reference 2 (Appendix A of the Summary Report).

4. VALIDATION OF THE [A] - MATRIX ROUTINE

To check out the computer program for the aerodynamic matrix, equation (23) was used to compute the pressure distribution for a highwing-midtail configuration, shown in Figure 5. Results were compared with those derived from a NASA Langley Vortex Lattice program, Reference 3.

Both programs employed a total of 80 panels with 50 panels on the halfwing, 10 on the half fuselage and 20 on one side of the tail. The pressure distributions are compared in Figure 6. Note that the computed ΔC_p is plotted at the panel centroid for the K.U. program, but at the panel quarter chord for the Vortex Lattice program. It is seen that the results from both programs agree reasonably well. The computation of stability derivatives is compared in Table 2. The experimental data are obtained from Reference 4. To determine the effect of the number of panels on the numerical outcome, 100 and 120 panel solutions were computed. Table 2. shows that there was little change by using a panel scheme of more than 100.

Table 2. Comparison of Computed Stability Derivatives with Experiment for the Configuration of Figure 5 at M = 0.25

	K.U. Program			Vortex Lattice Program	Experiment Reference 4
Derivatives	No. of panels			No. of panels	
	80	100	120	80	
C_{L_α} rad^{-1}	3.1930	3.105	3.0780	3.1208	3.28
dC_m / dC_L	-0.0395	-0.0541	-0.0429	-0.0438	-0.065

In comparison with experimental results, it is assumed that for a high wing configuration, the wing may be placed directly above the fuselage at a distance of one half fuselage diameter, so that two lifting surfaces (wing and fuselage) will overlap in some region. A similar aerodynamic representation has been assumed for a low wing configuration or for a high or low tail. Several other configurations presented in References 5 through 8 were investigated with the K.U. program. Their geometries are shown in Figures 7 through 10 respectively. The total number of panels used on a half configuration was 100. Table 3, shows the comparison with experimental results. It is seen that the computed results show reasonable agreement with experiments.

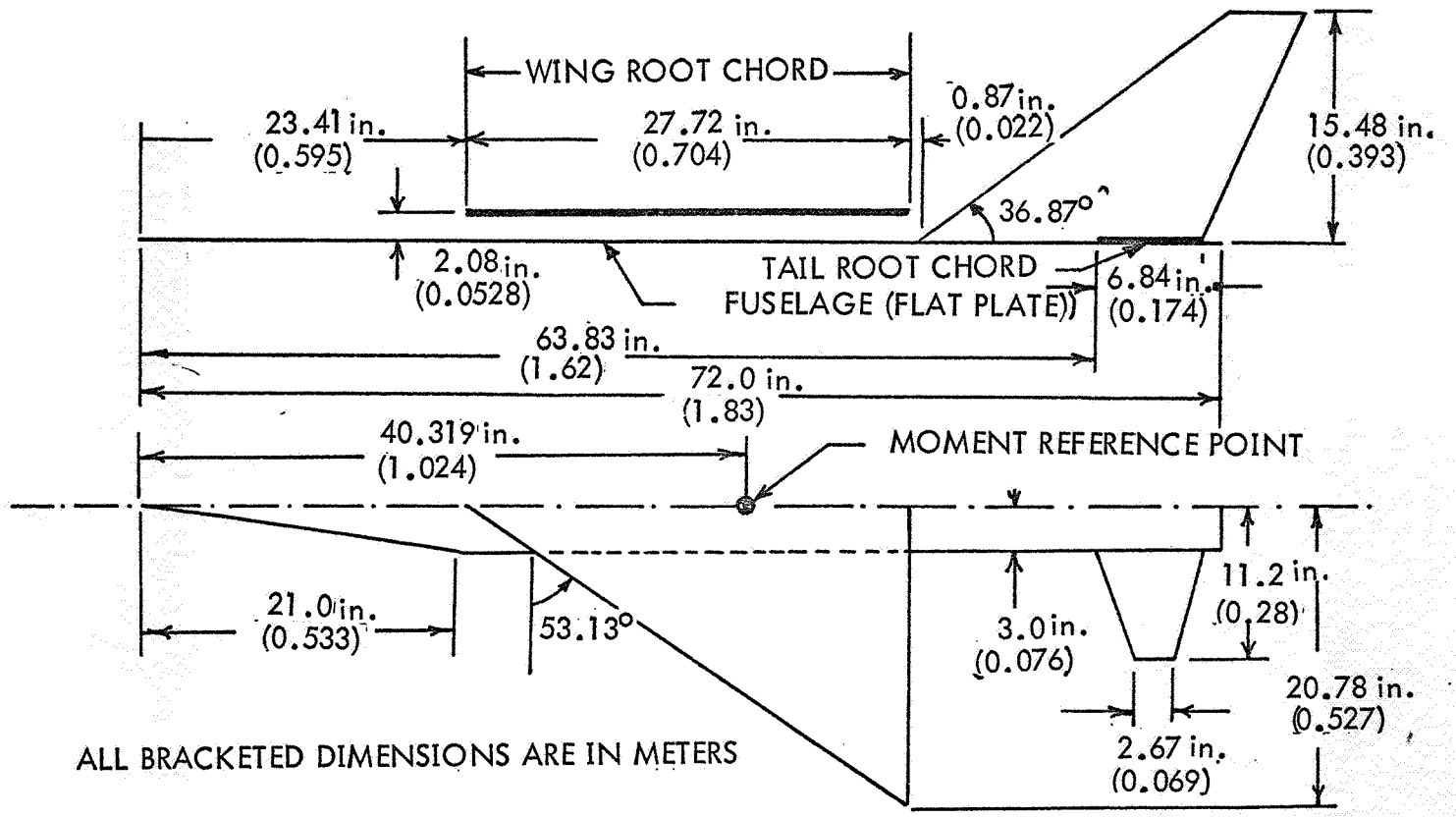

NOTE: CONFIGURATION WBH 1 OF REFERENCE 3

Figure 5 Geometry of a wing-body-tail configuration used for program checkout

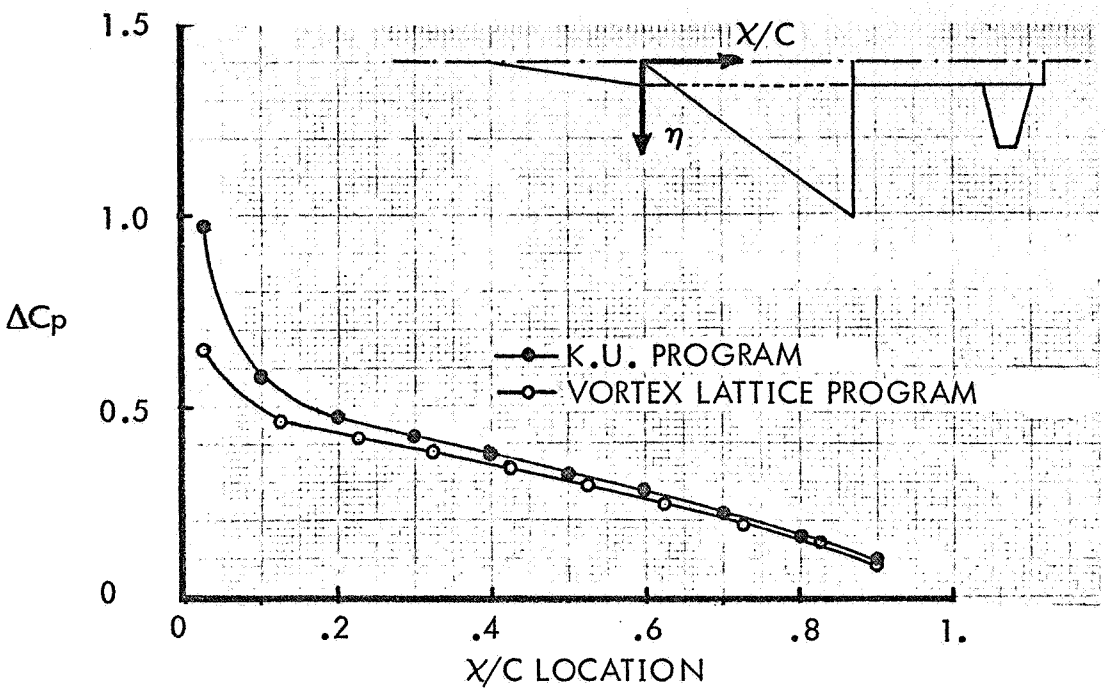

Figure 6a Comparison of wing pressure distribution at $\eta = 0.1$

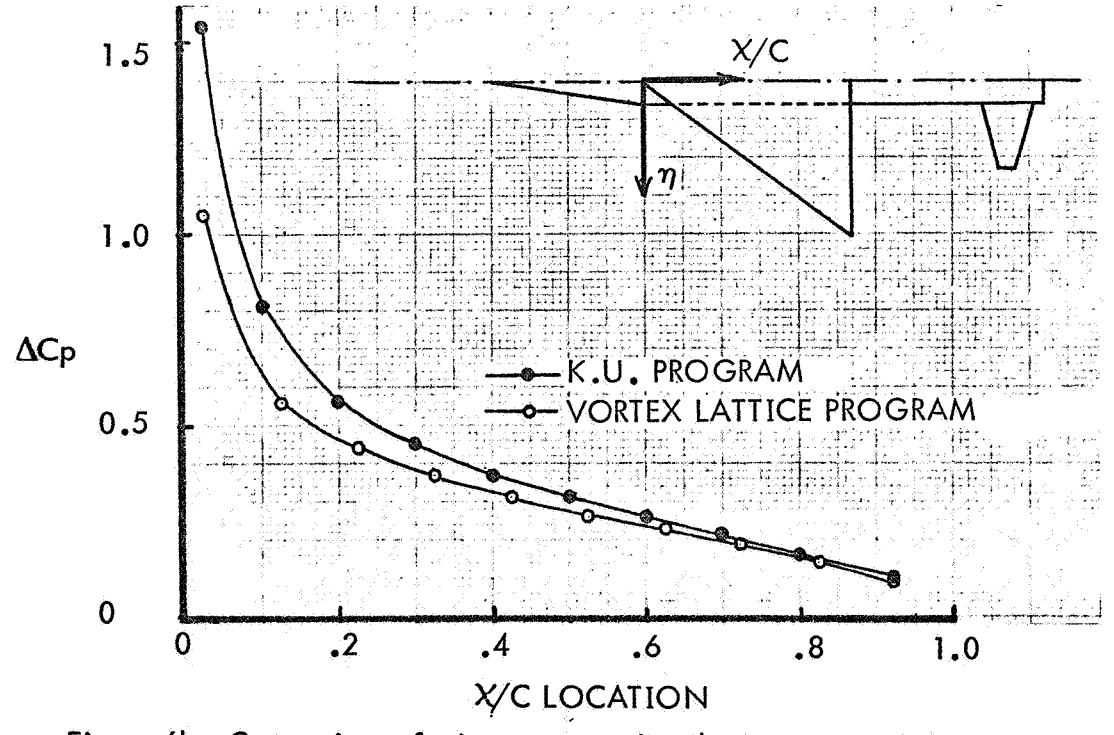

Figure 6b Comparison of wing pressure distribution at $\eta = 0.3$

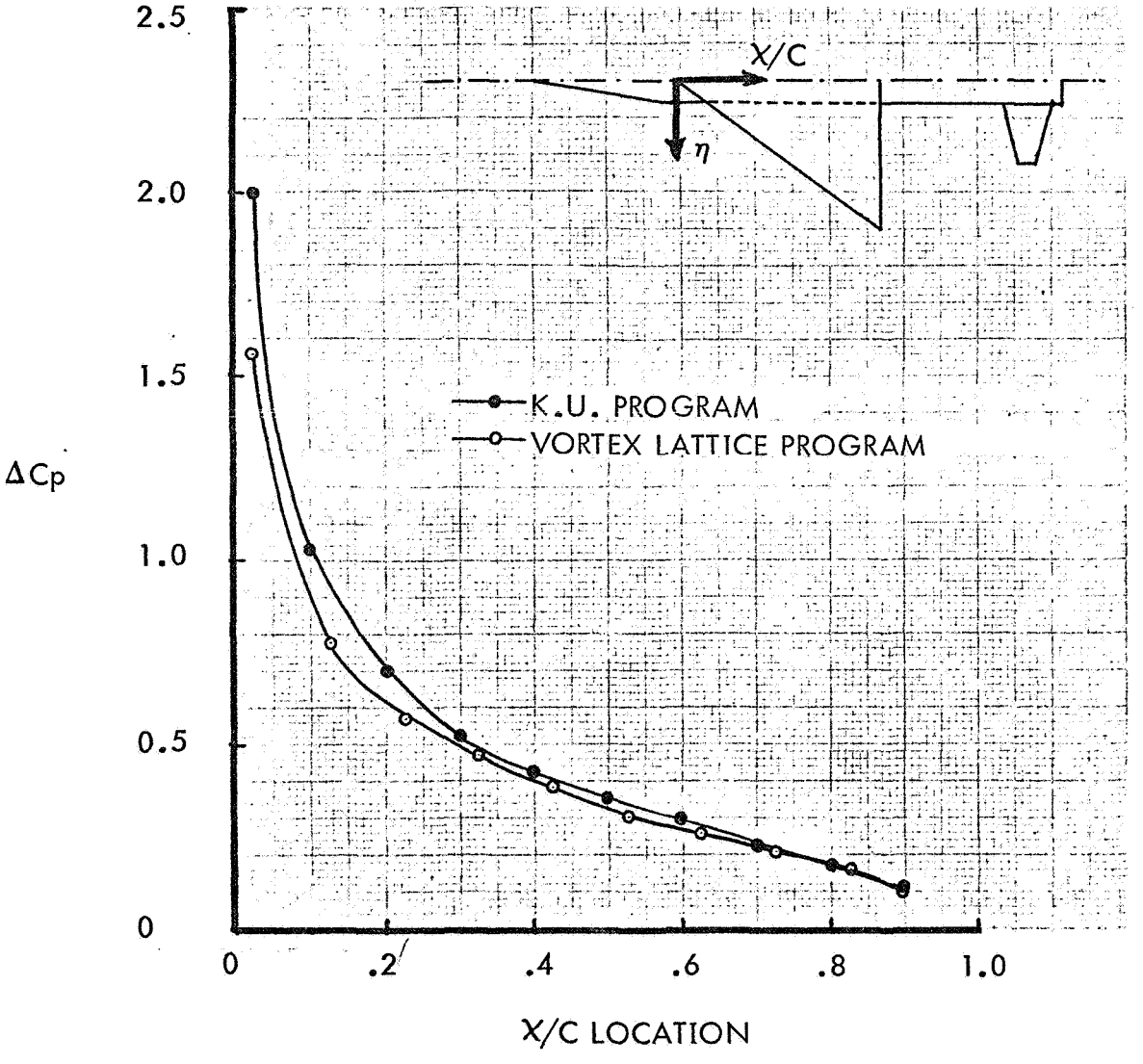

Figure 6c Comparison of wing pressure distribution at $\eta = 0.5$

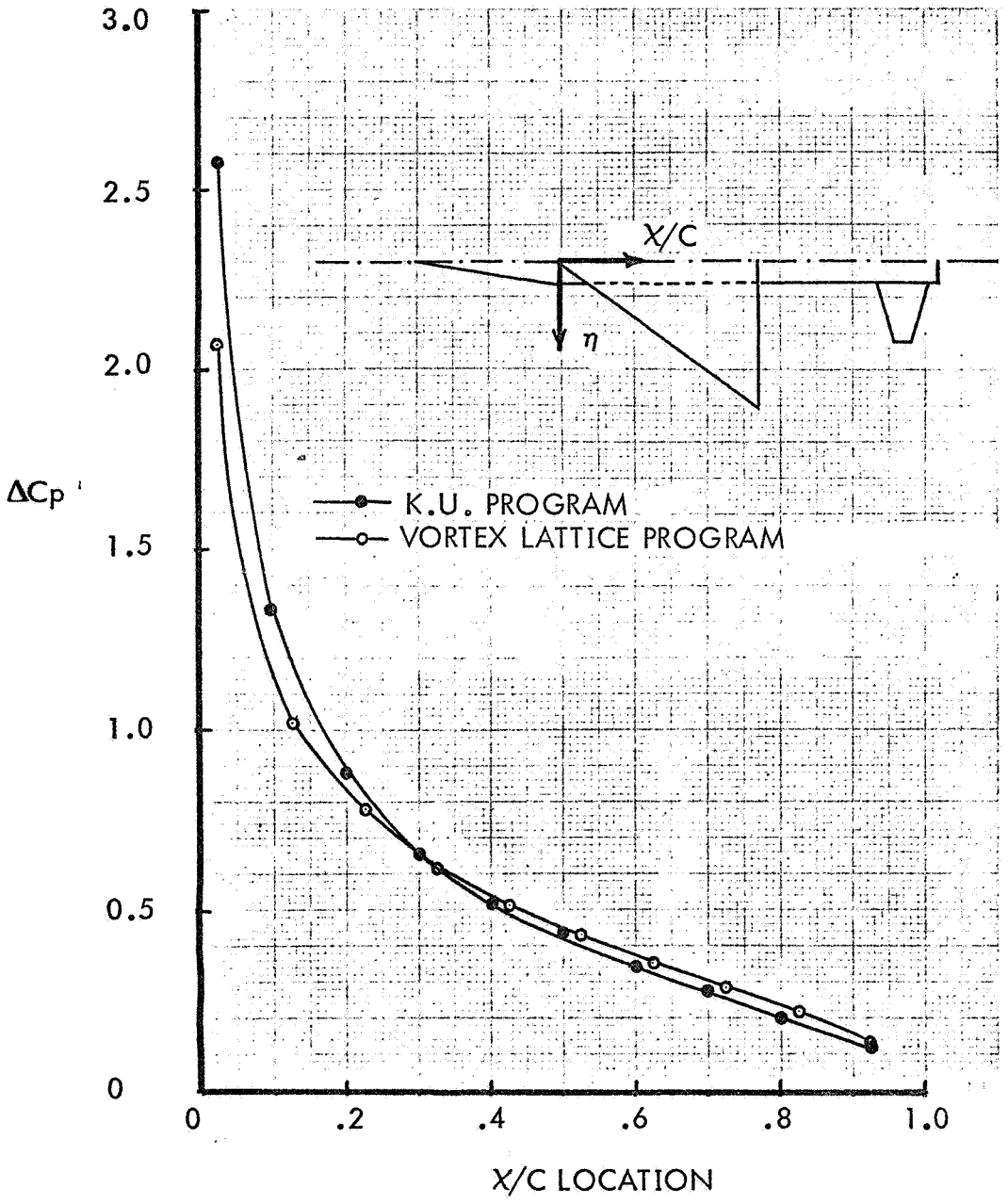

Figure 6d Comparison of Wing Pressure Distribution at $\eta = 0.7$

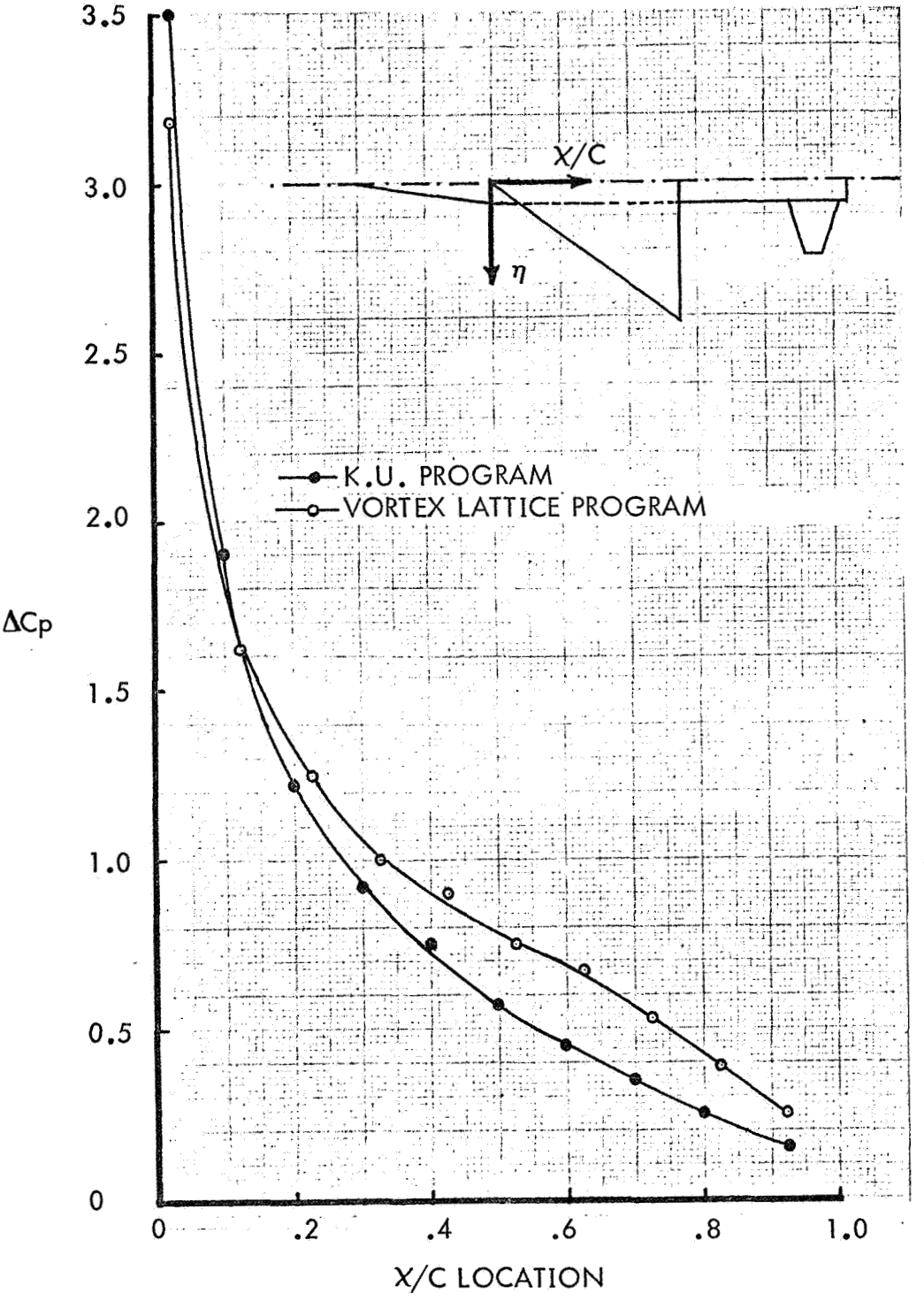

Figure 6e Comparison of wing pressure distribution at $\eta = 0.9$

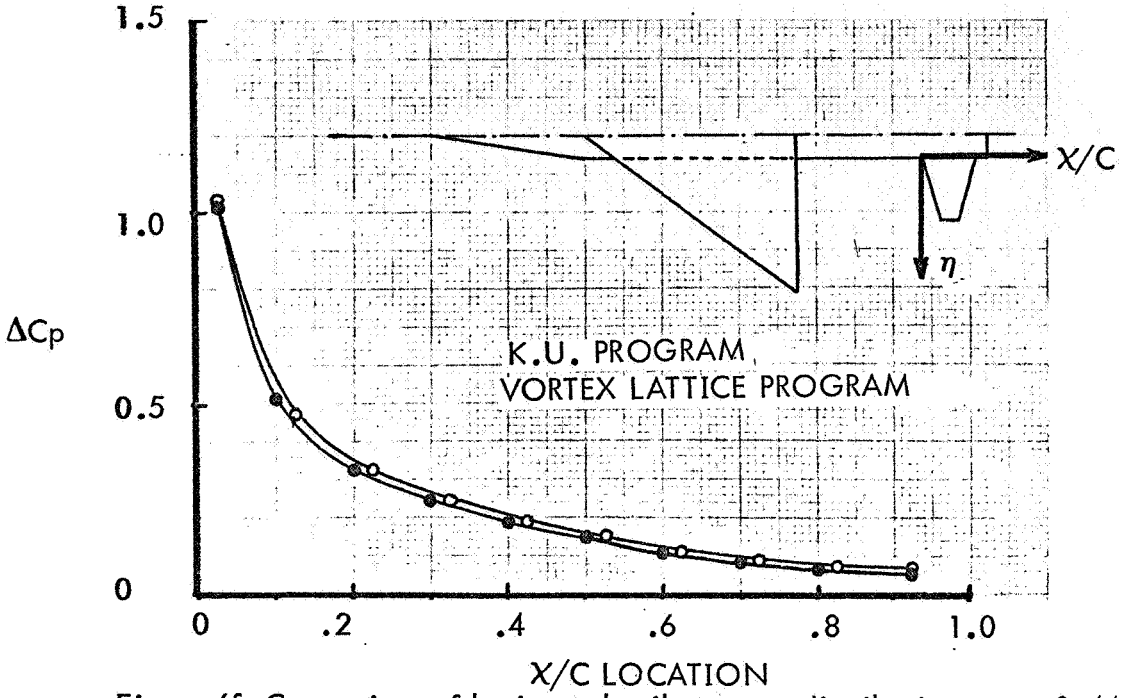

Figure 6f Comparison of horizontal tail pressure distribution at $\eta = 0.448$

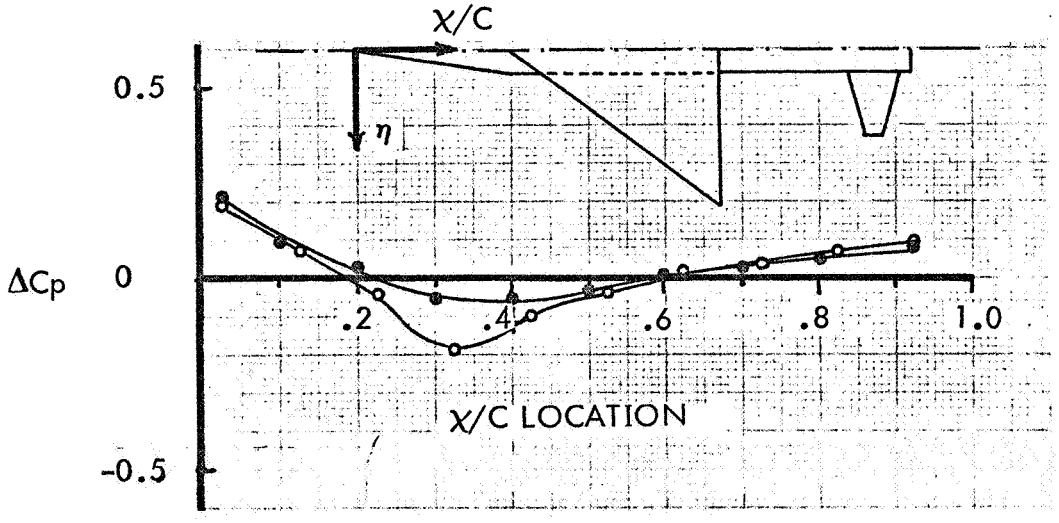

Figure 6g Comparison of fuselage pressure distribution at $\eta = 0.5$

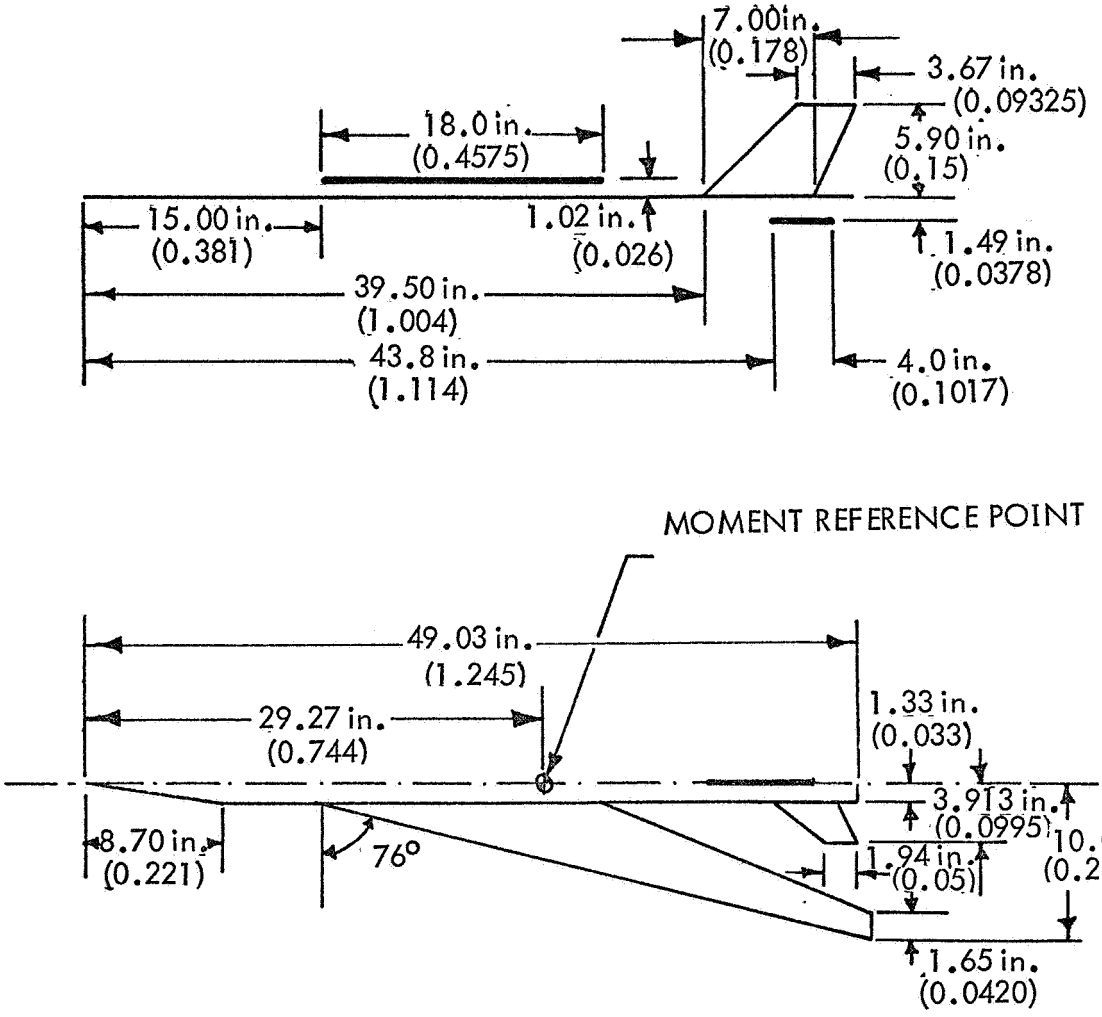

ALL BRACKETED DIMENSIONS IN METERS

NOTE: CONFIGURATION WBH 2 OF REFERENCE 5

Figure 7 Aerodynamic Representation for Geometry of WBH2

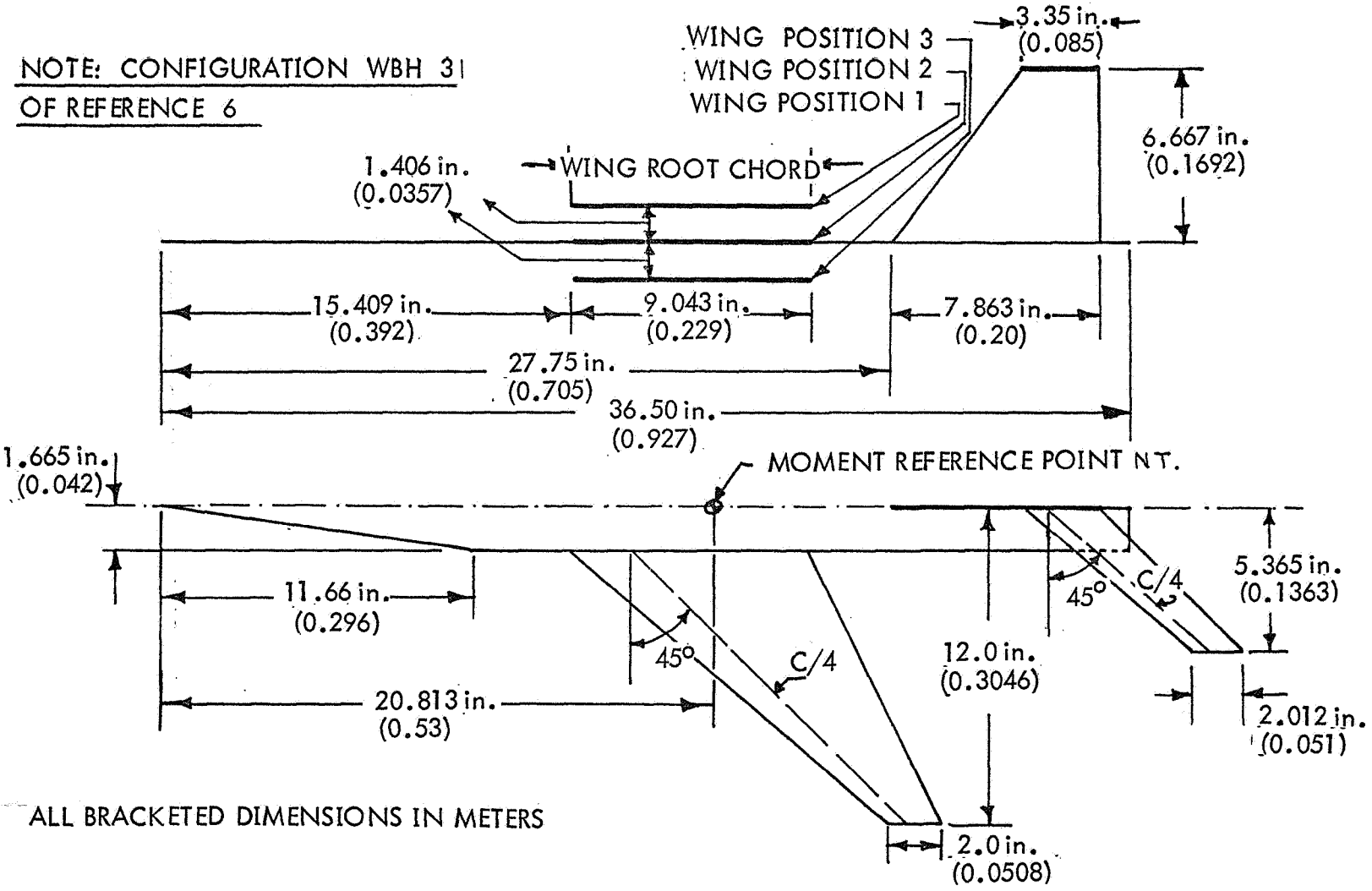

Figure 8 Aerodynamic Representation for Geometry of WBH 3

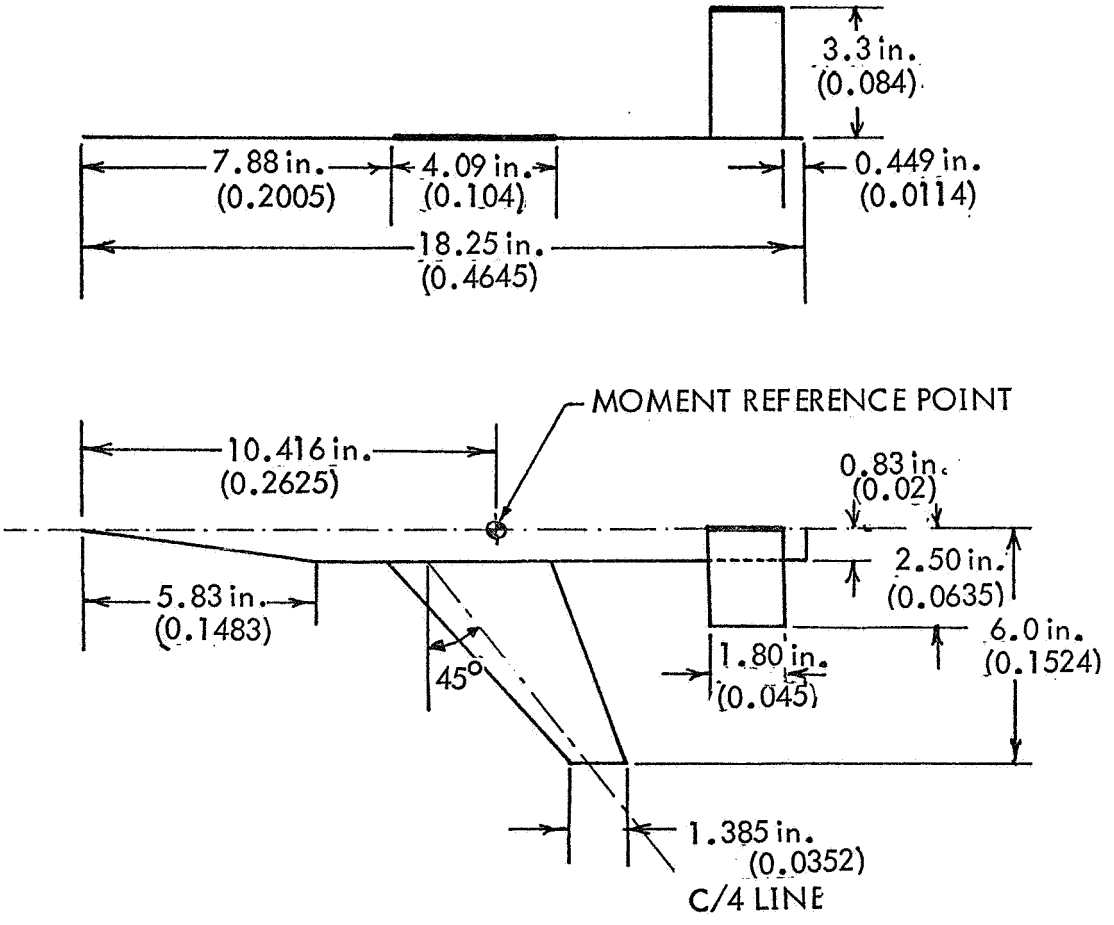

ALL BRACKETED DIMENSIONS IN METERS

NOTE: CONFIGURATION WBH 4 OF REFERENCE 7

Figure 9 Aerodynamic Representation for Geometry of WBH 4

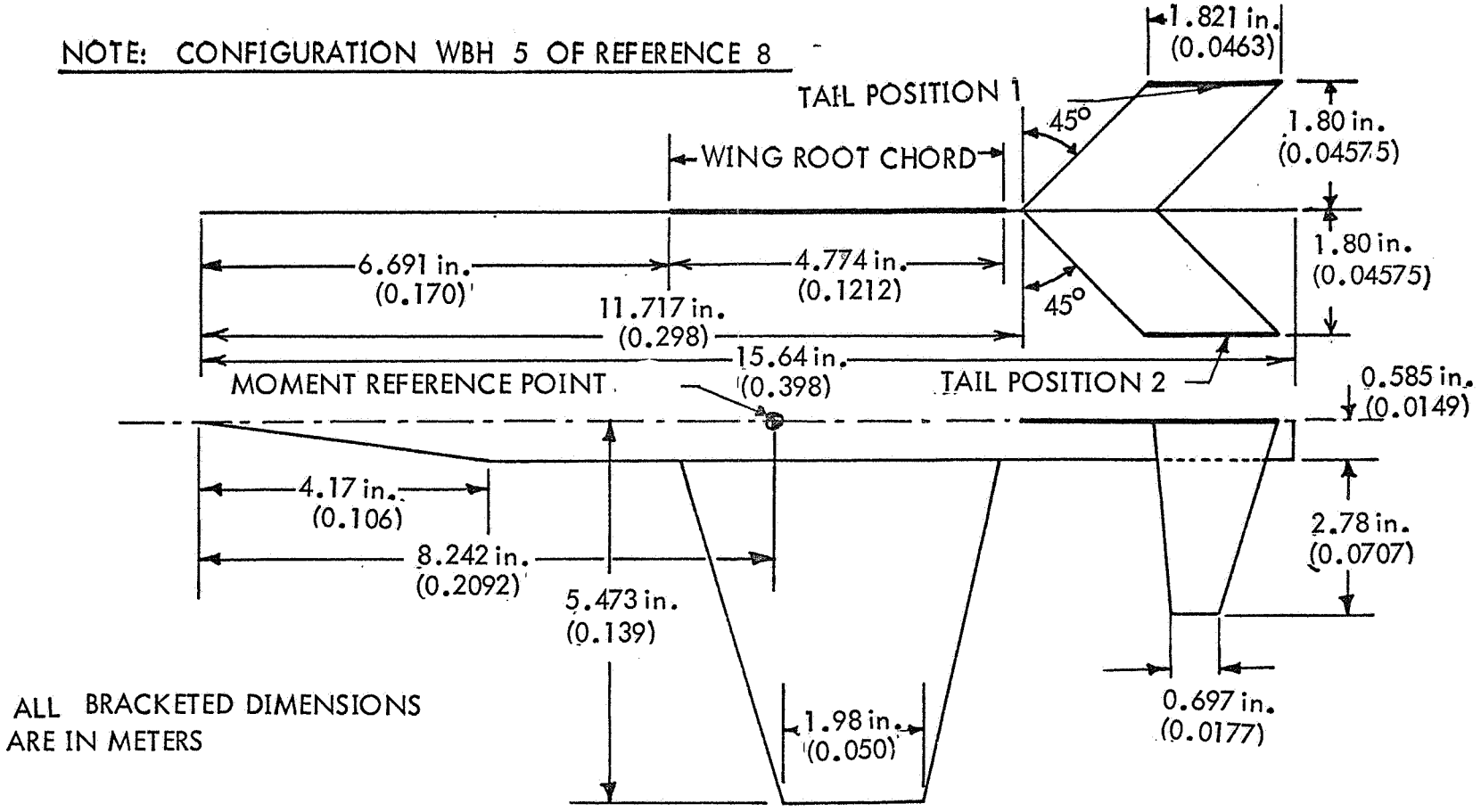

Figure 10 Aerodynamic Representation for Geometry of WBH 5

Table 3 Comparison of Computed Aerodynamic Characteristics with Experimental Results

WBH Number	Reference	Configuration	Mach No.	K.U. Program (100 panels)		Experimental	
				C_{L_α} rad^{-1}	dC_m/dC_L	C_{L_α} rad^{-1}	dC_m/dC_L
1	NACA TN 4041 Reference 4	Mid wing - Mid tail	0.25	2.9751	-0.07438	3.22	-0.06
		High wing - Mid tail	0.25	3.105	-0.0541	3.28	-0.065
		Mid wing - Low tail	0.60	3.24	-0.071	3.15	-0.075
2	NACA TN D-4076 Reference 5	High wing - Low tail	1.90	1.6559	-0.2756	1.59	-0.298
3	NACA RM L54L06 Reference 6	Low wing - High tail	2.01	2.751	-0.311	2.344	-0.308
		Mid wing - High tail	2.01	2.924	-0.397	2.344	-0.357
		High wing - High tail	2.01	3.066	-0.550	2.601	-0.561
4	NACA RM L57C08 Reference 7	Mid wing - High tail	0.60	4.560	-0.258	3.919	-0.258
5	NACA RM A57I10 Reference 8	Mid wing - Low tail	0.60	4.036	-0.1405	4.18	-0.16
		Mid wing - High tail	0.60	4.036	-0.1408	4.18	-0.13
		Mid wing - Low tail	1.40	4.356	-0.3907	4.41	-0.34
		Mid wing - High tail	1.40	4.356	-0.3905	4.13	-0.39

5. REFERENCES

1. Woodward, F.A., "Analysis and Design of Wing-Body Combinations at Subsonic and Supersonic Speeds," Journal of Aircraft, Vol. 5., No. 6, Nov. - Dec., 1968.

2. Roskam, J., Lan, C., and Mehrotra, S.; "A Computer Program for Calculating α- and q- Stability Derivatives and Induced Drag for Thin Elastic Aeroplanes at Subsonic and Supersonic Speeds," NASA CR-112229; Prepared by the Flight Research Laboratory of the University of Kansas under NASA Grant NGR 17-002-071, October, 1972. Appendix A of the Summary Report, NASA CR- 2117.

3. Margason, R.J. and Lamar, J.E., "Vortex-Lattice Fortran Program for Estimating Subsonic Aerodynamic Characteristics of Complex Planforms." NASA TN D-6142, 1971.

4. Tinling, E.T., and Lopez, A.E., "Subsonic Static Aerodynamic Characteristics of an Airplane Model Having a Triangular Wing of Aspect Ratio 3. I--Effects of Horizontal-tail location and size on the longitudinal characteristics." NACA TN 4041 , 1957.

5. Fuller, E.D., "Static Stability Characteristics at Mach Numbers from 1.90 to 4.63 of a 76° Swept Arrow Wing Model With Variations in Horizontal-Tail Height, Wing Height and Dihedral," NASA TN D-4076, 1967.

6. Spearman, M.L., et al., "Investigation of Aerodynamic Characteristics in Pitch and Sideslip of a 45° Swept-back-wing Airplane Model with Various Vertical Locations of Wing and Horizontal Tail," NACA RM L54L06, 1955.

7. Sleeman, W.C., Jr., "An Experimental Study at High Subsonic Speeds of Several Tail Configurations on a Model Having a 45° Sweptback Wing." NACA RM L57C08, 1957.

8. Stivers, L.S., Jr., and Lippmann, G.W., "Effects of Vertical Locations of Wing and Horizontal Tail on the Aerodynamic Characteristics in Pitch at Mach Numbers from 0.60 to 1.40 of an Airplane Configuration with an Unswept wing." NACA RM A57I10, 1957.